ADVANCED FUNCTIONAL MATERIALS
www.afm-journal.de

www.MaterialsViews.com

Engineering Efficiency Roll-Off in Organic Light-Emitting Devices

*Nicholas C. Erickson and Russell J. Holmes**

Previous studies have identified triplet-triplet annihilation and triplet-polaron quenching as the exciton density-dependent mechanisms which give rise to the efficiency roll-off observed in phosphorescent organic light-emitting devices (OLEDs). In this work, these quenching processes are independently probed, and the impact of the exciton recombination zone width on the severity of quenching in various OLED architectures is examined directly. It is found that in devices employing a graded-emissive layer (G-EML) architecture the efficiency roll-off is due to both triplet-triplet annihilation and triplet-polaron quenching, while in devices which employ a conventional double-emissive layer (D-EML) architecture, the roll-off is dominated by triplet-triplet annihilation. Overall, the efficiency roll-off in G-EML devices is found to be much less severe than in the D-EML device. This result is well accounted for by the larger exciton recombination zone measured in G-EML devices, which serves to reduce exciton density-driven loss pathways at high excitation levels. Indeed, a predictive model of the device efficiency based on the quantitatively measured quenching parameters shows the role a large exciton recombination zone plays in mitigating the roll-off.

1. Introduction

Organic light-emitting devices (OLEDs) are attractive for use in display and lighting applications due in part to high peak efficiency operation. One development which has enabled high peak external quantum efficiency (η_{EQE}) is the ability to harvest triplet excitons for electroluminescence (EL). The utilization of triplet excitons occurs via three pathways: (1) directly as radiative decay, i.e. electrophosphorescence,[1–5] or indirectly, from (2) triplet-triplet annihilation processes which result in the formation of a singlet exciton,[6–10] or (3) singlet states which are populated through reverse intersystem crossing from triplet states, as in thermally activated delayed fluorescence (TADF).[11–14] All of these routes, however, require population of the triplet exciton state through electrical excitation. Triplet excitons typically have long natural lifetimes, on the order of 10^{-6}–10^{-3}s.[2,15–17] A consequence of the long lifetime is that at the current densities often necessary to achieve high brightness levels, large triplet exciton densities are produced. These high densities result in exciton density-driven quenching processes, which are observed as a decrease in the η_{EQE} with increasing current density (and thus increasing brightness), a characteristic termed the "efficiency roll-off."[16,18–22] The efficiency roll-off is one factor which may limit the implementation of OLEDs in high brightness applications. Further, it has been suggested that device operating lifetimes may suffer in devices with a high degree of efficiency roll-off, as larger current densities are needed to reach high operating brightness levels.[22–26]

There are a variety of emissive layer architectures which have shown high peak efficiencies, including double-emissive layer (D-EML),[27–29] mixed-emissive layer (M-EML),[30–32] and graded-emissive layer (G-EML)[33–35] devices. The D-EML consists of two distinct layers, a hole transport material (HTM) and an electron transport material (ETM), both doped uniformly with a dilute emissive guest. This architecture can achieve a high degree of charge balance and strongly confines the charge carriers to a region near the HTM:ETM interface. The M-EML design consists of a uniformly mixed layer of HTM and ETM that is doped with the emissive guest. This design allows for the charge carrier mobilities of the composite layer to be tuned by varying the HTM:ETM ratio, ideally achieving ambipolar characteristics to maximize charge balance and efficient exciton formation.[30] The G-EML device is a single-layer device architecture which consists of a continuously varying composition profile, from nearly 100% HTM at the anode to nearly 100% ETM at the cathode, doped throughout with an emissive guest.[33] This device architecture has been previously used to achieve high η_{EQE} in red-, green-, and blue-light-emitting devices.[34]

Whereas the G-EML device may be optimized by tuning the composition gradient profile, the D-EML and M-EML device architectures often require the use of charge and exciton blocking and transport layers to achieve high peak performance. Device optimization is carried out by adjusting the doping concentration, thickness of each layer, and the overall HTM:ETM mixing ratio. These parameters are most often tuned to give low-voltage operation and high peak performance, though the impact these changes have on the spatial extent and location

N. C. Erickson
Department of Electrical and Computer Engineering
University of Minnesota
Minneapolis, MN 55455, USA
Prof. R. J. Holmes
Department of Chemical Engineering
and Materials Science
University of Minnesota
Minneapolis, MN 55455, USA
E-mail: rholmes@umn.edu

DOI: 10.1002/adfm.201401009

of the exciton recombination zone is rarely considered. The recombination zone width of D-EML and G-EML-based devices has previously been measured; it was found that the D-EML architecture had a significantly reduced width ($W \approx 15$ nm) compared to that of the G-EML device ($W \approx 80$ nm).[36] The G-EML device also shows a reduction in the efficiency roll-off compared to the D-EML device. Here, we quantitatively examine the exciton quenching processes present in both architectures using transient and steady state photo- and electro-luminescence measurements. All OLEDs and thin film test devices were fabricated using 4,4',4''-tris(carbazol-9-yl)triphenylamine (TCTA) as an HTM, 4,7-diphenyl-1,10-phenanthroline (BPhen) as an ETM, and the archetypal green phosphorescent molecule tris(2-phenylpyridine)iridium(III) ($Ir(ppy)_3$) as the emitter. The important quenching parameters are measured independently, and the impact of the recombination zone width on efficiency roll-off is examined directly and fully quantified.

2. Theory

2.1. Exciton Density-Driven Quenching

The physical processes responsible for exciton quenching in phosphorescent OLEDs have been previously identified as triplet-triplet annihilation between guest excitons and triplet-polaron quenching.[15,16,18,20,37,38] The impact of these two processes on the triplet exciton population can be written separately as:

$$\frac{dn_{ex}}{dt} = -\frac{n_{ex}}{\tau} - \frac{1}{2}\kappa_{TT} n_{ex}^2 + G \tag{1}$$

for triplet-triplet annihilation, and

$$\frac{dn_{ex}}{dt} = -\frac{n_{ex}}{\tau} - \kappa_{TP} \rho n_{ex} + G \tag{2}$$

for triplet-polaron quenching, where n_{ex} is the triplet exciton population, which may depend on position within the emissive layer, τ is the exciton lifetime, κ_{TT} is the rate of guest triplet-triplet annihilation, κ_{TP} is the rate of triplet-polaron annihilation, G is an exciton generation term, and ρ is the polaron density, which depends on position and which may be a function of the current density, J, or voltage, V, depending on the description of charge transport.[37,39,40] In Equation (2), the spatial overlap of polarons and excitons in the device is of particular importance. This property, however, is difficult to probe directly, thus the rate constant κ_{TP} reflects not only the strength of the interaction of polarons and excitons but also the spatial overlap.[16] Under device operating conditions, the exciton population becomes:[15,16]

$$\frac{dn_{ex}}{dt} = -\frac{n_{ex}}{\tau} - \frac{1}{2}\kappa_{TT} n_{ex}^2 - \kappa_{TP} \rho n_{ex} + \frac{J}{eW} \tag{3}$$

where the final term represents electrical generation of excitons, e is the elementary charge, and W is the width of exciton recombination zone in the device. Written this way, the generation term assumes all injected carriers form excitons, which may be the case for devices with a high degree of charge balance. Previously, loss of charge balance has been identified as a contributing factor to the efficiency roll-off observed in devices.[20] Loss of charge balance may be mitigated through device design, either by material selection or the incorporation of charge blocking layers. Whereas κ_{TT}, κ_{TP}, and τ are typically considered as material parameters that are independent of device design in typical OLED architectures, the exciton recombination zone in an OLED is dependent on the overlap of electron and hole charge densities, and thus is sensitive to the architecture of the device, particularly the emissive layer design. It is also worth noting that as written, Equation (3) does not include the quenching of excitons formed on the HTM or ETM. This assumption is reasonable as the host molecular orbital energy levels have been chosen to encourage exciton formation directly on the emissive guest under electrical excitation.

Under optical excitation, excitons are likely formed on the hosts, with host-guest energy transfer occurring rapidly and efficiently.[15] Assuming a high photoluminescence (PL) efficiency for emission,[41] the luminescent output, L, is linearly proportional to the exciton density ($L[t] \sim n_{ex}[t]/\tau$), Equation (1) may be solved to describe the transient decay of triplet guest excitons under optical excitation:

$$L[t] = \frac{L[t=0]}{\left(1 + \frac{\tau}{2} n_{ex}[0]\kappa_{TT} e^{\frac{t}{\tau}}\right) - \frac{\tau}{2} n_{ex}[0]\kappa_{TT}} \tag{4}$$

where $n_{ex}[0]$ is the initial population of excitons, and is calculated from measurements of the initial laser pulse energy, spot size, and the Beer-Lambert law using the optical absorption coefficients of each sample.

To realize an independent measurement of the exciton-polaron interaction, Equation (2) may be solved in the steady-state:

$$L[V] = \frac{L[V=0]}{1 + \tau\kappa_{TP}\rho[V]} \tag{5}$$

Here, the polaron density, $\rho[V]$, is described as a function of applied voltage. Theoretically, the charge carrier density (and equivalently, the polaron density) may be predicted from the applied voltage, V (and consequently applied field, assumed to be uniform across the device thickness, d, $F = V/d$), in a device operating in the injection-limited current (ILC) regime.[42] This model has been previously used to describe single-carrier devices with contacts which inject and extract either electrons-only, or holes-only.[39] Under a continuous-wave optical pump and an applied DC voltage, the PL of a single-carrier D-EML or G-EML device (see Methods section) is given by Equation (5).

A steady-state solution to Equation (3) may be found which describes the photon output per electron input, which is equivalent to the external quantum efficiency, η_{EQE}. That solution, after Reineke et al., is:[16]

$$\frac{\eta_{EQE}}{\eta_o} = \Theta\left(\sqrt{\frac{\Delta^2 + \Gamma\kappa_{TT}}{\kappa_{TT}^2}} - \frac{\Delta}{\kappa_{TT}}\right) \tag{6}$$

with

$$\Theta = \frac{eW}{\tau J} \tag{7}$$

$$\Delta = \left(\frac{1}{\tau} + \kappa_{TP} C J^{1/(l+1)} \right) \tag{8}$$

and

$$\Gamma = \frac{2J}{eW} \tag{9}$$

where a relationship between the current density and polaron density in a full device is assumed, $\rho = CJ^{1/(l+1)}$; C is a constant which describes the electronic properties of the device, and l is taken to be unity.[16]

3. Results and Discussion

3.1. Characterization of Triplet-Triplet Annihilation

The normalized transient PL decay of each materials system and the corresponding fits using Equation (4) are shown in **Figures 1**a-c for multiple initial exciton densities. In all material systems, an initial fast decay is observed which increases in severity with increasing excitation density. This feature is attributed to strong exciton-exciton quenching at high exciton densities. As the exciton population falls at longer times, due to both radiative decay and quenching events, exciton-exciton interactions decrease and the decay is dominated by the natural exciton lifetime. The κ_{TT} and τ extracted for each system vary only within experimental error, and have average values of $\kappa_{TT} = (1.9 \pm 4.1) \times 10^{-12}$ cm^3 s^{-1} and $\tau = (1.62 \pm 0.19) \times 10^{-6}$ s. The average used here as κ_{TT} reflects the interaction of the emissive guest with itself; these values are in good agreement with previous data reported for Ir(ppy)$_3$-based systems.[15,16,43]

3.2. Characterization of Triplet-Polaron Quenching

With τ determined from previous measurements, κ_{TP} may be extracted independently, without the need to correct for triplet-triplet annihilation, which is independent of the polaron density. Plots of the steady-state PL as a function of polaron density are shown in **Figure 2**a for D-EML and Figure 2b for G-EML, hole-only devices. As the polaron density is increased, a clear decrease in steady-state PL is observed, indicating significant exciton-polaron quenching. Electric field-induced exciton quenching has been previously suggested as a loss pathway; however, such effects are typically observed only at very high fields ($F > 2.5$ MV/cm),[16,44] greater than those used in the present study ($F < 2.0$ MV/cm). Interestingly, the values of κ_{TP} extracted for D-EML and G-EML devices are similar, $\kappa_{TP} = (6.3 \pm 4.7)$v $\times 10^{-13}$ cm^{3}s^{-1} and $\kappa_{TP} = (2.8 \pm 1.6) \times 10^{-13}$, respectively. These values are in good agreement with those previously reported by Reineke et al. for TCTA:Ir(ppy)$_3$ devices.[16] In that work, the single-carrier devices were designed to be in the space-charge limited current (SCLC) regime and the polaron density was related to the current density in a trap-filling SCLC model.[16]

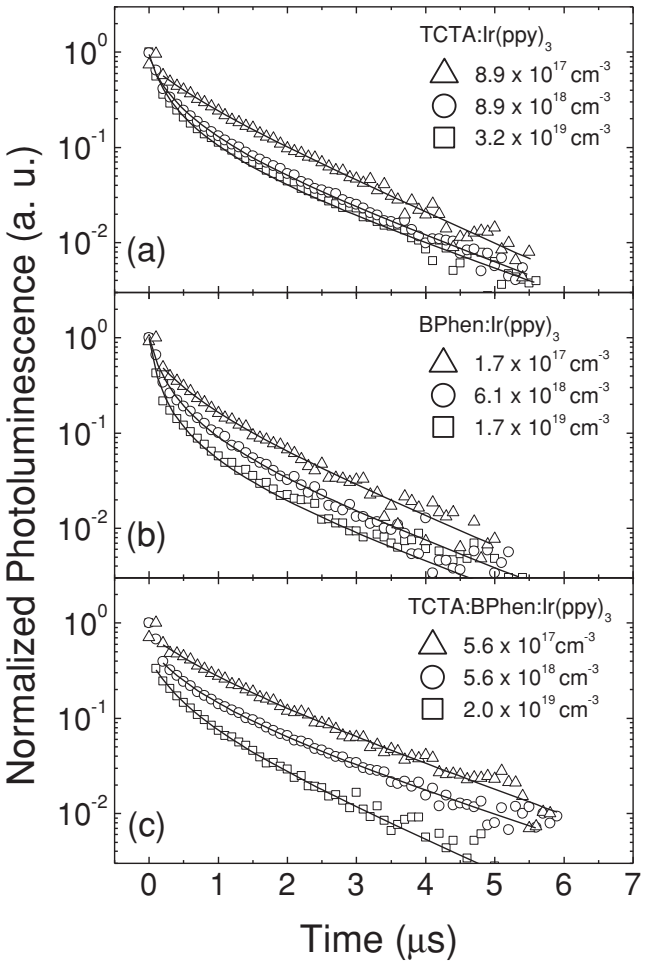

Figure 1. Transient photoluminescence decays for 30-nm-thick films of (a) TCTA:2 wt.% Ir(ppy)$_3$, (b) BPhen:2 wt.% Ir(ppy)$_3$ and (c) TCTA:BPhen:2 wt.% Ir(ppy)$_3$ at different initial exciton densities. Fits to Equation (4) for each measurement are shown as solid lines.

3.3. Efficiency roll-off in D-EML and G-EML OLEDs

To characterize the efficiency roll-off in full devices, optimized D-EML OLEDs were fabricated with the following structure: ITO (150 nm)/TCTA:5 wt.% Ir(ppy)$_3$ (40 nm)/BPhen:5 wt.% Ir(ppy)$_3$ (40 nm)/LiF (1 nm)/Al (100 nm). Optimized G-EML OLEDs had a structure of: ITO (150 nm)/[TCTA:BPhen]:2 wt.% Ir(ppy)$_3$ G-EML (1:1 gradient profile, 100 nm)/LiF (1 nm)/Al (100 nm).[33,34] The current density-voltage and brightness-voltage characteristics for each of the devices are shown in **Figures 3**a and 3c, respectively. The corresponding peak-normalized η_{EQE} for the devices are shown versus current density in Figures 3b and 3d for D-EML and G-EML devices, respectively; the peak η_{EQE} of the D-EML device is $\eta_{EQE} = 11.3\%$, while the G-EML device reaches a peak $\eta_{EQE} = 16.3\%$. The best-fits of Equation (6) to each device are also shown in Figures 3b

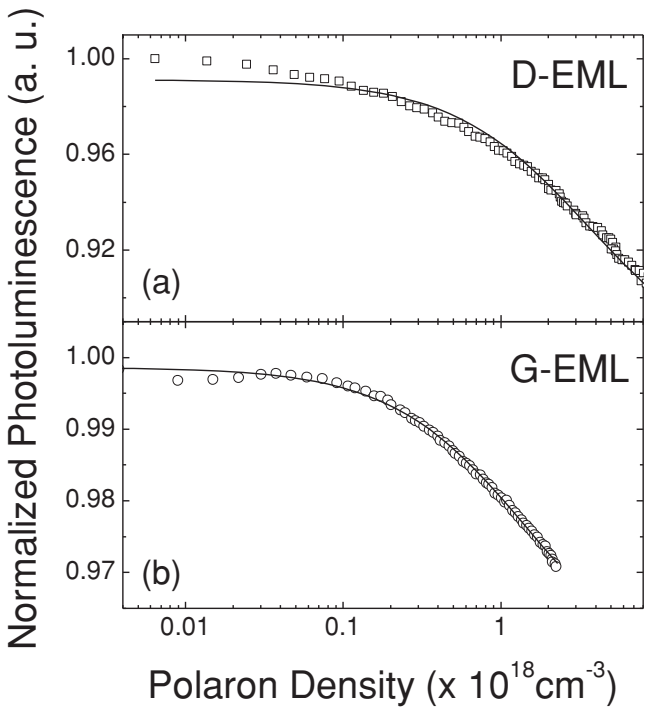

Figure 2. Steady-state photoluminescence of (a) D-EML and (b) G-EML hole-only devices as a function of polaron density. Fits to Equation (5) are shown as solid lines for each device.

Table 1. Measured and best fit rate constants for triplet-triplet annihilation (κ_{TT}) and triplet-polaron quenching (κ_{TP}) for D-EML and G-EML OLEDs with the measured exciton lifetime (τ), and measured recombination zone width (W) of each device.

	κ_{TT} (cm^3 s^{-1})	κ_{TP} (cm^3 s^{-1})	τ (s)	W (nm)
D-EML (Measured)	1.9×10^{-12}	6.3×10^{-13}	1.62×10^{-6}	15
D-EML (Best Fit)	2.1×10^{-12}	0		
G-EML (Measured)	1.9×10^{-12}	2.8×10^{-13}		80
G-EML (Best Fit)	5.7×10^{-12}	2.8×10^{-13}		

and 3d (solid line); the model parameters for each fit are shown in **Table 1**. To compare the roll-off of devices with different peak η_{EQE}, the current density at which the efficiency decreases to half of its maximum, termed "J_0," is noted, J_0 = 170 mA cm^{-2} for the D-EML and J_0 = 325 mA cm^{-2} for the G-EML. As has been observed previously, the G-EML device exhibits significantly less efficiency roll-off than the D-EML device.[36]

For the G-EML device, best-fits of Equation (6) were achieved by allowing κ_{TT} and κ_{TP} to vary; the resulting values are *within* the experimental error bars, indicating the high degree of accuracy with which the model (and measured values of W, κ_{TT}, κ_{TP}, and τ) reproduces the measured η_{EQE}. In the case of the D-EML device, the best-fit κ_{TT} constant is also within experimental error, see Table 1. However, the best-fit value of κ_{TP} for the D-EML devices is essentially zero, in contrast to the

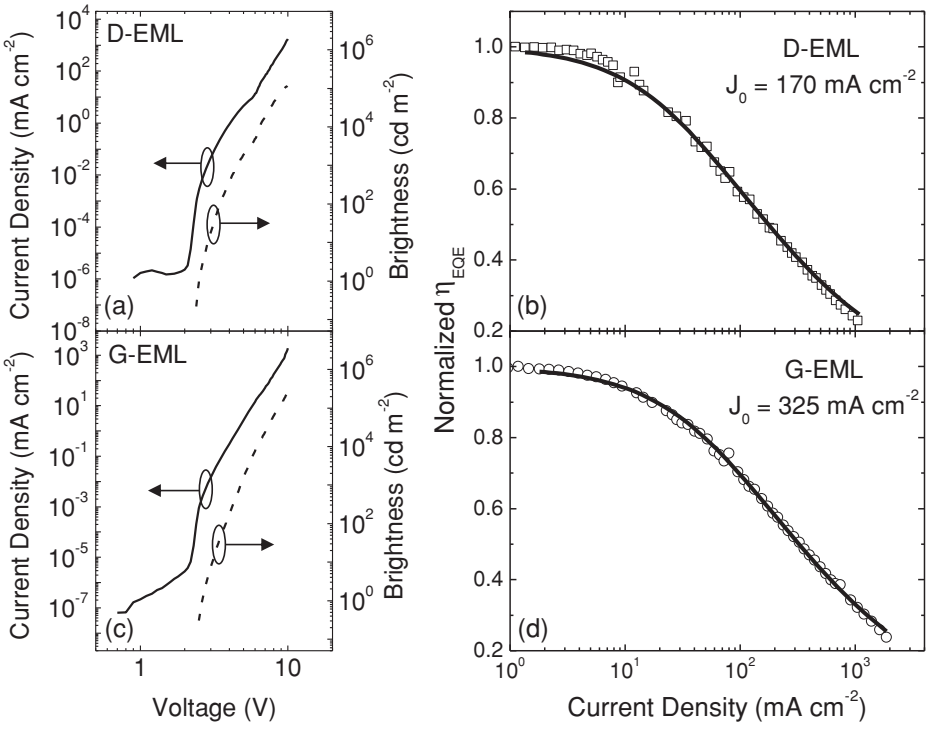

Figure 3. (a) Current density-voltage, brightness-voltage and (b) normalized η_{EQE} for the D-EML device. (c) Current density-voltage, brightness-voltage and (d) normalized η_{EQE} for the G-EML device. Fits to Equation (6) of the η_{EQE} for each device are shown as solid lines. The J_0 of each device is noted, J_0 = 170 mA cm^{-2} for the D-EML device and J_0 = 325 mA cm^{-2} for the G-EML device.

measured value of κ_{TP} from the above experiments. This discrepancy likely arises from the different distributions of excitons and polarons within the test films compared to actual devices. In the test films, excitons are created throughout the film, according to the optical field distribution and the absorption properties of the materials; however, according to previous work on the D-EML device,[36] excitons are only present near the HTM:ETM interface. That work ascribed the narrow recombination zone in D-EML devices to the short distance that minority carriers penetrate into the opposing host layer, likely by transport along the guest. In the low concentrations used in the D-EML device, efficient charge transport along the guest is unlikely. The narrow recombination zone likely results in a much lower exciton-polaron density overlap in the actual D-EML device, which in turn reduces the best-fit value of κ_{TP}, which, in the framework of Equation (2), reflects both the interaction and spatial overlap of excitons and polarons. To verify this, the steady-state PL of hole-only devices with an alternate D-EML structure of: ITO (150 nm)/TCTA (45 nm)/TCTA:5 wt.% $Ir(ppy)_3$ (5 nm)/BPhen:5 wt.% $Ir(ppy)_3$ (5 nm)/UGH2 (45 nm)/Au (50 nm), where UGH2 is the wide-energy-gap molecule: 1,4-bis(triphenylsilyl)benzene, was also examined.[4] In this configuration, excitons are only generated in the narrow region of the device containing $Ir(ppy)_3$. In this device, no decrease in steady-state PL was observed with polaron densities up to 10^{19} cm^{-3}, giving $\kappa_{TP} \approx 0$, consistent with the fits of device η_{EQE}. Clearly, both triplet-triplet annihilation and triplet-polaron quenching are processes which affect the roll-off of G-EML devices, while the roll-off of the D-EML device is dominated by triplet-triplet annihilation. In both cases, the recombination zone width is fixed to experimentally-measured values, and, given the good agreement of the η_{EQE} data and fits to Equation (6), is a key parameter in determining the efficiency roll-off.

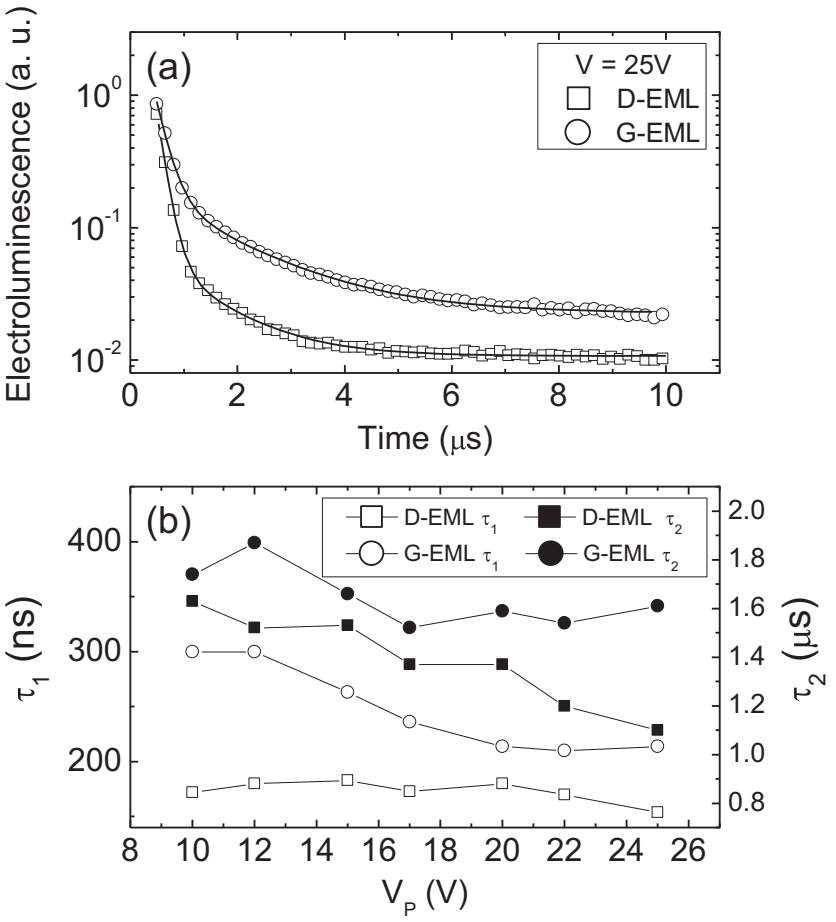

Figure 4. (a) Transient electroluminescence decays for D- EML (squares) and G-EML (circles) devices for a voltage pulse of 250 ns, with a peak voltage, V = 25 V. Biexponential fits to the transient decay of each device are shown as solid lines. (b) Transient fit lifetimes, τ_1 (open) and τ_2 (closed) as a function of voltage for D-EML (squares) and G-EML (circles).

3.4. Transient Measurements of OLED Electroluminescence

The cumulative effects of triplet-triplet annihilation and triplet-polaron quenching can also be observed in transient EL. These quenching processes lead to a reduction in the total exciton lifetime, particularly under high excitation. Transient EL may therefore be used to show the impact of recombination zone width on the quenching processes in an OLED. Voltage pulses with a width of 250 ns and period of 200 μs were applied to D-EML and G-EML devices with a variable peak voltage, V, and the resulting transient EL decays are shown in **Figure 4**a for V = 25 V. Previously, transient EL decays have been fit using biexponential equations with short and long lifetimes, τ_1 and τ_2, respectively. The short lifetime has been previously associated with host-guest interactions, while the long lifetime has been associated with guest exciton decay.[15] The fitted values of τ_1 and τ_2 are shown in Figure 4b over a range of voltages for both D-EML and G-EML devices. For low peak voltage pulses, both devices approach a common value of τ_2 which is in close agreement with the lifetime value measured in the PL transient experiments. At high peak voltage pulses, the value of τ_2 decreases drastically in the D-EML device relative to the G-EML device. The longer-lived EL transients of the G-EML devices, compared to the D-EML devices, indicate the role the wide recombination zone plays in mitigating the exciton density-dependent quenching effects.

3.5. Predicting η_{EQE} roll-off in OLEDs

Given the good fits obtained using Equation (6) and the efficiency roll-off of the G-EML devices, it is instructive to predict the efficiency roll-off of G-EML devices with a range of

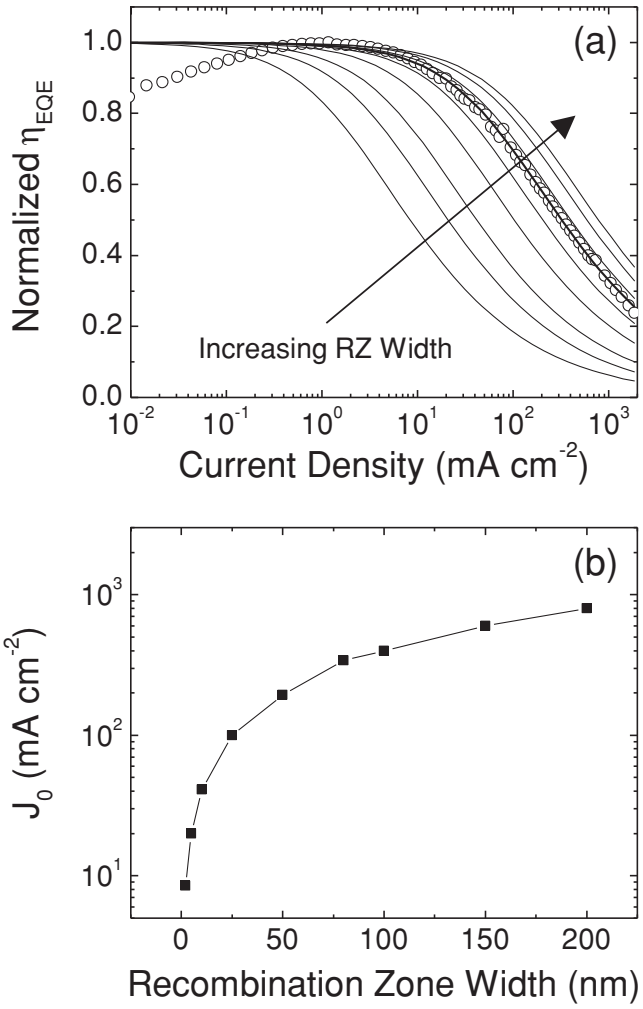

Figure 5. (a) Normalized η_{EQE} for G-EML devices with varying recombination zone widths, as predicted from Equation (6). Measured data for the G-EML device used in the present study is shown (circles) together with the best fit to Equation (6). (bold line). (b) The J_0 of each predicted device is shown versus recombination zone width.

recombination zone widths, keeping κ_{TT}, κ_{TP}, and τ fixed to the measured values. **Figure 5**a shows the efficiency roll-off of G-EML devices having recombination zone widths which vary from 2–200 nm, together with the η_{EQE} of the reported G-EML device. To compare the devices, the predicted J_0 of each device is plotted versus recombination zone width in Figure 5b. As seen in Figure 5b, there is a sharp increase in J_0 for a moderate increase in W, particularly for low recombination zone widths. For devices like the D-EML-based OLEDs with inherently small recombination zones, engineering a small improvement in recombination zone width may have a large impact on the efficiency roll-off. In G-EML OLEDs, increases in thickness to further expand the recombination zone must be balanced by potential increases in resistance and driving voltage. It is expected that this optimization will be facilitated by further engineering the composition gradient in thick layers. In all OLEDs, engineering the recombination zone width, while maintaining charge and exciton confinement, offers a route towards improving the efficiency roll-off in OLEDs.

4. Conclusion

In summary, the four main parameters which impact efficiency roll-off in OLEDs (κ_{TT}, κ_{TP}, τ, and W) have been measured independently for D-EML and G-EML devices. A model of the efficiency roll-off which is based on those parameters was used to accurately predict the performance of the OLEDs of interest. In the case of the G-EML device, it was found that the η_{EQE} is well-predicted by measured values of κ_{TT} and κ_{TP}, with the recombination zone fixed according to previous experimental results. In the D-EML device, the η_{EQE} was best-predicted using only κ_{TT}, with $\kappa_{TP} \sim 0$. These results indicate that triplet-triplet annihilation and triplet-polaron quenching are processes which impact the efficiency roll-off of G-EML devices, while the D-EML device efficiency roll-off is dominated by triplet-triplet annihilation. Further, the G-EML device exhibited significantly less efficiency roll-off, due in large part to the wide recombination zone present in that device. Model predictions of the efficiency roll-off of G-EML devices, with fixed quenching parameters κ_{TT}, κ_{TP}, and τ, were shown to depend strongly on the exciton recombination zone width. In the future, the G-EML device architecture may offer a route towards engineering efficient, single-layer OLEDs which have large recombination zones, thus reducing the efficiency roll-off and extending the range of useful brightness levels in OLED applications.

5. Experimental Section

Organic light-emitting devices were fabricated on glass substrates coated with a 150-nm-thick layer of indium-tin oxide (ITO) having a sheet resistance of 15 Ω/□. Substrates were cleaned and treated in UV-ozone ambient prior to film deposition. All organic layers were grown using vacuum thermal sublimation (<10^{-7} Torr) without breaking vacuum. Devices were defined by evaporating a cathode consisting of a 1-nm-thick layer of LiF and a 100-nm-thick layer of Al through a shadow mask with 1 mm diameter openings. The D-EML devices had the following structure: ITO (150 nm)/TCTA:5 wt.% $Ir(ppy)_3$ (40 nm)/BPhen:5 wt.% $Ir(ppy)_3$ (40 nm)/LiF (1 nm)/Al (100 nm). Optimized G-EML devices had a structure of: ITO (150 nm)/[TCTA:BPhen]:2 wt.% $Ir(ppy)_3$ G-EML (1:1 gradient profile, 100 nm)/LiF (1 nm)/Al (100 nm).[33] Films for transient PL measurements were deposited on pre-cleaned glass substrates for each host:guest combination of interest. Hole-only single carrier devices were fabricated on pre-cleaned glass substrates with ITO as a bottom contact and Au as a top contact.

Transient PL experiments were conducted using a pulsed nitrogen laser (Optical Building Blocks) with an excitation wavelength of λ = 337 nm, a pulse length of approximately 1 ns. The laser spot size was limited by an iris diaphragm to a diameter of 2 mm at the sample. The laser pulse energy was measured using a Coherent EnergyMax 10MB-HE powermeter. The pulse energy was measured to be 33.1 μJ at the sample surface. The transient PL signal was collected with a set of lenses and focused down on to a fast photodiode (Thorlabs PDA10A). The photodiode signal was recorded using a 1GHz bandwidth oscilloscope (Tektronix TDS5104b). Transient EL experiments were conducted using a pulse generator (HP 8114a) and the collection setup described above. For the steady-state PL quenching experiments, an LED laser with a pump wavelength λ = 405 nm (B&W Tek 405–40E) was used to excite the samples, while a large-area silicon photodiode was used to detect the emission (Hamamatsu S3584–08).

Acknowledgments

This work was supported primarily by the National Science Foundation (NSF) MRSEC Program under Award No. DMR-0819885. Support was also received from the University of Minnesota Initiative for Renewable Energy and the Environment.

Received: March 29, 2014
Revised: May 20, 2014
Published online: July 24, 2014

[1] M. A. Baldo, S. Lamansky, P. E. Burrows, M. E. Thompson, S. R. Forrest, *Appl. Phys. Lett.* **1999**, *75*, 4.
[2] M. A. Baldo, D. F. O'Brien, Y. You, A. Shoustikov, S. Sibley, M. E. Thompson, S. R. Forrest, *Nature* **1998**, *395*, 151.
[3] D. Tanaka, H. Sasabe, Y.-J. Li, S.-J. Su, T. Takeda, J. Kido, *Jpn. J. Appl. Phys. 2-Lett. Express Lett.* **2007**, *46*, L10.
[4] R. J. Holmes, B. W. D'Andrade, S. R. Forrest, X. Ren, J. Li, M. E. Thompson, *Appl. Phys. Lett.* **2003**, *83*, 3818.
[5] N. Chopra, J. Lee, Y. Zheng, S.-H. Eom, J. Xue, F. So, *Appl. Phys. Lett.* **2008**, *93*, 143307.
[6] J. Partee, E. L. Frankevich, B. Uhlhorn, J. Shinar, Y. Ding, T. J. Barton, *Phys. Rev. Lett.* **1999**, *82*, 3673.
[7] D. Yokoyama, Y. Park, B. Kim, S. Kim, Y.-J. Pu, J. Kido, J. Park, *Appl. Phys. Lett.* **2011**, *99*, 123303.
[8] Z. D. Popovic, H. Aziz, *J. Appl. Phys.* **2005**, *98*, 013510.
[9] D. Y. Kondakov, *J. Appl. Phys.* **2007**, *102*, 114504.
[10] D. Y. Kondakov, T. D. Pawlik, T. K. Hatwar, J. P. Spindler, *J. Appl. Phys.* **2009**, *106*, 124510.
[11] Q. Zhang, J. Li, K. Shizu, S. Huang, S. Hirata, H. Miyazaki, C. Adachi, *J. Am. Chem. Soc.* **2012**, *134*, 14706.
[12] H. Uoyama, K. Goushi, K. Shizu, H. Nomura, C. Adachi, *Nature* **2012**, *492*, 234.
[13] A. Endo, K. Sato, K. Yoshimura, T. Kai, A. Kawada, H. Miyazaki, C. Adachi, *Appl. Phys. Lett.* **2011**, *98*, 083302.
[14] K. Masui, H. Nakanotani, C. Adachi, *Org. Electron.* **2013**, *14*, 2721.
[15] M. A. Baldo, C. Adachi, S. R. Forrest, *Phys. Rev. B* **2000**, *62*, 10967.
[16] S. Reineke, K. Walzer, K. Leo, *Phys. Rev. B* **2007**, *75*, 125328.
[17] R. J. Holmes, S. R. Forrest, Y.-J. Tung, R. C. Kwong, J. J. Brown, S. Garon, M. E. Thompson, *Appl. Phys. Lett.* **2003**, *82*, 2422.
[18] J. Kalinowski, W. Stampor, J. Mężyk, M. Cocchi, D. Virgili, V. Fattori, P. Di Marco, *Phys. Rev. B* **2002**, *66*, 235321.
[19] D. Song, S. Zhao, Y. Luo, H. Aziz, *Appl. Phys. Lett.* **2010**, *97*, 243304.
[20] N. C. Giebink, S. R. Forrest, *Phys. Rev. B* **2008**, *77*, 235215.
[21] M.-T. Lee, J.-S. Lin, M.-T. Chu, M.-R. Tseng, *Appl. Phys. Lett.* **2009**, *94*, 083506.
[22] C. Murawski, K. Leo, M. C. Gather, *Adv. Mater.* **2013**, *25*, 6801.
[23] K. T. Kamtekar, A. P. Monkman, M. R. Bryce, *Adv. Mater.* **2010**, *22*, 572.
[24] P. Wellmann, M. Hofmann, O. Zeika, A. Werner, J. Birnstock, R. Meerheim, G. He, K. Walzer, M. Pfeiffer, K. Leo, *J. Soc. Inf. Disp.* **2005**, *13*, 393.
[25] M. C. Gather, S. Köber, S. Heun, K. Meerholz, *J. Appl. Phys.* **2009**, *106*, 024506.
[26] R. Meerheim, S. Scholz, S. Olthof, G. Schwartz, S. Reineke, K. Walzer, K. Leo, *J. Appl. Phys.* **2008**, *104*, 014510.
[27] G. He, M. Pfeiffer, K. Leo, M. Hofmann, J. Birnstock, R. Pudzich, J. Salbeck, *Appl. Phys. Lett.* **2004**, *85*, 3911.
[28] X. Zhou, D. S. Qin, M. Pfeiffer, J. Blochwitz-Nimoth, A. Werner, J. Drechsel, B. Maennig, K. Leo, M. Bold, P. Erk, H. Hartmann, *Appl. Phys. Lett.* **2002**, *81*, 4070.
[29] S.-J. Su, E. Gonmori, H. Sasabe, J. Kido, *Adv. Mater.* **2008**, *20*, 4189.
[30] M. E. Kondakova, T. D. Pawlik, R. H. Young, D. J. Giesen, D. Y. Kondakov, C. T. Brown, J. C. Deaton, J. R. Lenhard, K. P. Klubek, *J. Appl. Phys.* **2008**, *104*, 094501.
[31] J.-H. Lee, C.-I. Wu, S.-W. Liu, C.-A. Huang, Y. Chang, *Appl. Phys. Lett.* **2005**, *86*, 103506.
[32] J. Lee, J.-I. Lee, J. Y. Lee, H. Y. Chu, *Appl. Phys. Lett.* **2009**, *94*, 193305.
[33] N. C. Erickson, R. J. Holmes, *Appl. Phys. Lett.* **2010**, *97*, 083308.
[34] N. C. Erickson, R. J. Holmes, *J. Appl. Phys.* **2011**, *110*, 084515.
[35] S. Lee, C. W. Tang, *J. Vac. Sci. Technol. B Microelectron. Nanometer Struct.* **2011**, *29*, 062401.
[36] N. C. Erickson, R. J. Holmes, *Adv. Funct. Mater.* **2013**, *23*, 5190.
[37] S. Reineke, G. Schwartz, K. Walzer, K. Leo, *Phys. Status Solidi RRL Rapid Res. Lett.* **2009**, *3*, 67.
[38] W. Staroske, M. Pfeiffer, K. Leo, M. Hoffmann, *Phys. Rev. Lett.* **2007**, *98*, 197402.
[39] Z. B. Wang, M. G. Helander, M. T. Greiner, J. Qiu, Z. H. Lu, *J. Appl. Phys.* **2010**, *107*, 034506.
[40] M. A. Lampert, P. Marks, *Current Injection in Solids* Academic Press Inc, New York **1970**.
[41] Y. Kawamura, K. Goushi, J. Brooks, J. J. Brown, H. Sasabe, C. Adachi, *Appl. Phys. Lett.* **2005**, *86*, 071104.
[42] J. C. Scott, G. G. Malliaras, *Chem. Phys. Lett.* **1999**, *299*, 115.
[43] J. Kalinowski, J. Mężyk, F. Meinardi, R. Tubino, M. Cocchi, D. Virgili, *J. Appl. Phys.* **2005**, *98*, 063532.
[44] R. Kersting, U. Lemmer, M. Deussen, H. J. Bakker, R. F. Mahrt, H. Kurz, V. I. Arkhipov, H. Bässler, E. O. Göbel, *Phys. Rev. Lett.* **1994**, *73*, 1440.